THE JOURNAL OF BIOLOGICAL CHEMISTRY VOL. 286, NO. 34, pp. 29941–29950, August 26, 2011

Crystal Structure of H_2O_2-dependent Cytochrome $P450_{SP\alpha}$ with Its Bound Fatty Acid Substrate

INSIGHT INTO THE REGIOSELECTIVE HYDROXYLATION OF FATTY ACIDS AT THE α POSITION[*S]

Received for publication, March 30, 2011, and in revised form, June 22, 2011 Published, JBC Papers in Press, June 30, 2011, DOI 10.1074/jbc.M111.245225

Takashi Fujishiro[‡1], Osami Shoji[‡], Shingo Nagano[§], Hiroshi Sugimoto[¶], Yoshitsugu Shiro[¶], and Yoshihito Watanabe[‖2]

From the [‡]Department of Chemistry, Graduate School of Science, Nagoya University, Furo-cho, Chikusa-ku, Nagoya 464-8602, Japan, [§]Department of Chemistry and Biotechnology, Graduate School of Engineering, Tottori University, 4-101 Koyama-Minami, Tottori 680-8550, Japan, [¶]RIKEN SPring-8 Center Harima Institute, 1-1-1 Kouto, Mikazuki-cho, Sayo, Hyogo 679-5148, Japan, and [‖]Research Center for Materials Science, Nagoya University, Furo-cho, Chikusa-ku, Nagoya 464-8602, Japan

Cytochrome $P450_{SP\alpha}$ (CYP152B1) isolated from *Sphingomonas paucimobilis* is the first P450 to be classified as a H_2O_2-dependent P450. $P450_{SP\alpha}$ hydroxylates fatty acids with high α-regioselectivity. Herein we report the crystal structure of $P450_{SP\alpha}$ with palmitic acid as a substrate at a resolution of 1.65 Å. The structure revealed that the C_α of the bound palmitic acid in one of the alternative conformations is 4.5 Å from the heme iron. This conformation explains the highly selective α-hydroxylation of fatty acid observed in $P450_{SP\alpha}$. Mutations at the active site and the F–G loop of $P450_{SP\alpha}$ did not impair its regioselectivity. The crystal structures of mutants (L78F and F288G) revealed that the location of the bound palmitic acid was essentially the same as that in the WT, although amino acids at the active site were replaced with the corresponding amino acids of cytochrome $P450_{BS\beta}$ (CYP152A1), which shows β-regioselectivity. This implies that the high regioselectivity of $P450_{SP\alpha}$ is caused by the orientation of the hydrophobic channel, which is more perpendicular to the heme plane than that of $P450_{BS\beta}$.

Cytochrome P450s (P450s)[3] are ubiquitous heme-containing monooxygenases that play crucial roles in the oxidative metabolism of many exogenous and endogenous compounds (1–4). X-ray crystal structure analysis is one of the most powerful methods for visualizing the structures of P450s and their interactions with substrates in the heme cavity at the atomic level. Since the first crystal structure of P450, $P450_{cam}$ (CYP101A1) was reported by Poulos *et al.* (5), the crystal structures of P450s from mammals (6–14), archaea (15–17), and bacteria (18–27) have been reported, and interactions between their substrates and amino acid residues at substrate recognition sites have been clarified. Most P450s accomplish monooxygenation by reductive activation of molecular oxygen using NADPH or NADH to produce compound I (oxoferryl porphyrin π cation radical). P450s also use H_2O_2 to generate compound I, but the efficiency of this reaction is poor compared with that of reductive activation of molecular oxygen. In 1994, Matsunaga *et al.* (28) isolated $P450_{SP\alpha}$ (CYP152B1) from *Sphingomonas paucimobilis* and reported that it exclusively uses H_2O_2 as the oxidant and catalyzes α-selective (100%) hydroxylation of long alkyl chain fatty acids (29). Although $P450_{SP\alpha}$ is the first P450 to be classified as a family of H_2O_2-dependent P450, its crystal structure has not been determined despite its potential as a biocatalyst. The first crystal structure of H_2O_2-dependent P450, $P450_{BS\beta}$ (CYP152A1), which has 44% amino acid identity to $P450_{SP\alpha}$, was reported in 2003 by Lee *et al.* (30). The crystal structure of a substrate-bound form of $P450_{BS\beta}$ (Protein Data Bank code 1IZO) revealed that $P450_{BS\beta}$ lacks general acid-base residues around the distal side of the heme, although this arrangement is highly conserved among peroxidases and peroxygenases (31–35). Instead of the general acid-base residues, the terminal carboxylate group of the bound fatty acid interacts with the guanidinium group of Arg^{242} located near the heme group. The distance between an oxygen atom of the carboxylate group of palmitic acid and the heme iron is 5.3 Å, which is similar to that observed in chloroperoxidase (CPO) from *Caldariomyces fumago*; the distance between an oxygen atom of glutamic acid side chain and the heme iron is 5.1 Å (34, 35). The location of the carboxylate group of palmitic acid bound to $P450_{BS\beta}$ suggests that the general acid-base function for the facile formation of compound I is accomplished by the carboxylate group

* This work was supported by Grant-in-Aid for Scientific Research (S) 19105044 (to Y. W.), Grant-in-Aid for Scientific Research on Innovative Areas 22105012 (to Y. S.), and Grant-in-Aid for Young Scientists (A) 21685018 (to O. S.) from the Ministry of Education, Culture, Sports, Science, and Technology (Japan).

[S] The on-line version of this article (available at http://www.jbc.org) contains supplemental text, references, and Figs. S1–S5.

The atomic coordinates and structure factors (codes 3AWM, 3AWQ, and 3AWP) have been deposited in the Protein Data Bank, Research Collaboratory for Structural Bioinformatics, Rutgers University, New Brunswick, NJ (http://www.rcsb.org/).

[1] Supported by Japan Society for the Promotion of Science Research Fellowships for Young Scientists.

[2] To whom correspondence should be addressed: Research Center for Materials Science, Nagoya University, Furo-cho, Chikusa-ku, Nagoya 464-8602, Japan. Tel./Fax: 81-52-789-3557; E-mail: yoshi@nucc.cc.nagoya-u.ac.jp.

[3] The abbreviations used are: P450, cytochrome P450; $P450_{SP\alpha}$, cytochrome P450 isolated from *S. paucimobilis* (CYP152B1); $P450_{BS\beta}$, cytochrome P450 isolated from *Bacillus subtilis* (CYP152A1); P450BM3, cytochrome P450 isolated from *Bacillus megaterium* (CYP102A1); $P450_{cam}$, cytochrome P450 isolated from *Pseudomonas putida* (CYP101A1); MPD, (±)-2-methyl-2,4-pentanediol; MES, 2-(*N*-morpholino)ethanesulfonic acid; β-OH C_{14}, β-hydroxymyristic acid; α-OH C_{14}, α-hydroxymyristic acid; C_{14}, myristic acid; CPO, chloroperoxidase.

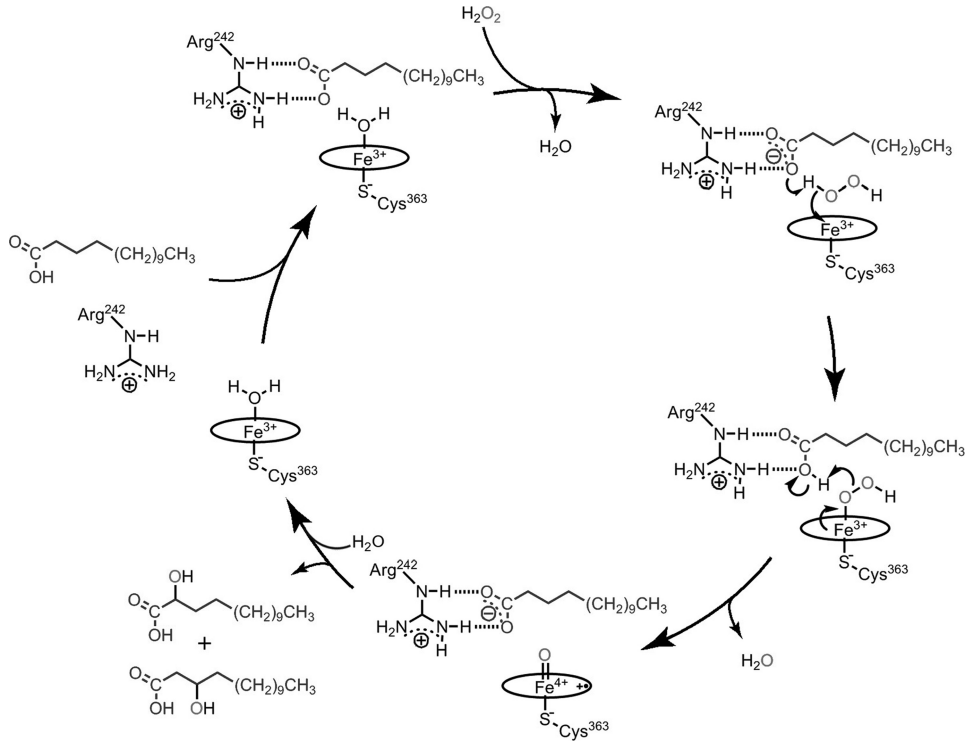

SCHEME 1. **A proposed catalytic reaction mechanism for hydroxylation of long alkyl chain fatty acid.** For the generation of compound I (oxoferryl porphyrin π-cation radical), the carboxylate group of the fatty acid (*blue*) that serves as a general acid-base catalyst first accepts a proton from H_2O_2, producing the ferric hydroperoxy complex (Fe^{+3}-OOH). Subsequently, a proton is donated to the distal oxygen atom of the ferric hydroperoxy complex followed by the O–O bond cleavage to produce compound I.

of the substrate (Scheme 1). Recently, we have shown that $P450_{BS\beta}$ is able to catalyze H_2O_2-dependent monooxygenation of foreign compounds such as styrene and ethylbenzene in the presence of a carboxylic acid with a short alkyl chain (C_4–C_{10}), a so-called "decoy molecule" (36). The crystal structure of a heptanoic acid (C_7)-bound form of $P450_{BS\beta}$ was analyzed, and an interaction between Arg^{242} and the carboxylate group of heptanoic acid was detected. We also resolved the crystal structure of the substrate-free form of $P450_{BS\beta}$ and found that binding of fatty acid or substrate analogues did not induce any notable structural change, whereas the substrate-free form of $P450_{BS\beta}$ never reacts with H_2O_2 (37). These observations further confirm that substrate binding initiates the formation of compound I via a salt bridge between Arg^{242} and the carboxylate group at the active site.

$P450_{BS\beta}$ oxidizes the α- and β-positions of fatty acids in a 40:60 ratio, whereas $P450_{SP\alpha}$ exclusively oxidizes the α position. To elucidate the cause of this selectivity, we need to study the crystal structures of both enzymes. Although the crystal structure of the substrate-bound form of $P450_{BS\beta}$ is known, that of $P450_{SP\alpha}$ has not been resolved. Therefore, we crystallized $P450_{SP\alpha}$ and succeeded in preparing high quality crystals of $P450_{SP\alpha}$. Herein we describe the x-ray crystal structure of $P450_{SP\alpha}$ containing a fatty acid at a resolution of 1.65 Å and examine enzymatic properties of its mutants to study its highly selective α-hydroxylation of fatty acids. We also compare the structure of $P450_{SP\alpha}$ with that of $P450_{BS\beta}$ in the context of similarities and differences among H_2O_2-dependent P450s.

EXPERIMENTAL PROCEDURES

Crystallization of $P450_{SP\alpha}$—$P450_{SP\alpha}$ WT was concentrated to 13.4 mg/ml in 50 mM MES (pH 7.0) containing 20% (v/v) glycerol by centrifugation using Amicon Ultra filter units (Millipore, Co.). A 2-μl aliquot of the concentrated $P450_{SP\alpha}$ solution was mixed with 2 μl of a reservoir solution composed of 0.1 M HEPES (pH 7.0) and 35% (v/v) MPD. Crystals of $P450_{SP\alpha}$ were grown by a sitting-drop vapor diffusion method at 20 °C for 6 days. The $P450_{SP\alpha}$ L78F and F288G mutants were crystallized under the same conditions used for the WT.

Data Collection, Phasing, and Refinement of $P450_{SP\alpha}$—Crystals were flash-cooled in liquid nitrogen. X-ray diffraction data sets were collected on a beam line BL41XU instrument equipped with an ADSC Quantum 315 CCD detector at the RIKEN SPring-8 (Hyogo, Japan) with a 1.0 Å wavelength at 100 K. The HKL2000 (38) program was used for integration of diffraction intensities and scaling. Initial phases were calculated and refined using the SHELXE program (39) and the hkl2map graphical interface (40). In the calculated electron density, the main chain was clearly traceable, and the initial polypeptide chain was built using ARP/wARP (41). Model building and refinement were performed using COOT (42), CNS (43), and REFMAC5 (44). TLS refinement (45) was performed in the final stages of the refinement, defining each chain in the asymmetric unit as a separate TLS group. The resulting model had a final R_{fact} of 15.1% and an R_{free} of 17.3% (Table 1). The final model consisted of one polypeptide chain with residues 9–415 of $P450_{SP\alpha}$, one heme, one palmitic acid, one MPD, and 371 water molecules. Structure validation was performed using

TABLE 1
Data collection and refinement statistics

	WT	L78F	F288G
Data collection			
Wavelength (Å)	1.000	1.000	1.000
Space group	$P3_121$	$P3_121$	$P3_121$
Cell dimensions			
a, *b*, *c* (Å)	94.440, 94.440, 113.553	94.137, 94.137, 113.402	94.58, 94.58, 113.449
α, β, γ (°)	90.000, 90.000, 120.000	90.000, 90.000, 120.000	90.000, 90.000,120.000
Resolution (Å)	50.00-1.68 (1.68-1.65)	20.0-1.90 (1.97-1.90)	20.0-1.80 (1.86-1.80)
No. of total observed reflections	1,516,965	493,946	582,013
No. of unique reflections	70,272	46,225	54,812
R_{merge} (%)[a,b]	6.4 (48.9)	7.5 (38.0)	6.2 (34.9)
Completeness (%)[a]	99.1 (82.8)	100.0 (100.0)	99.9 (100.0)
$I/\sigma(I)$[a]	84.5 (6.2)	31.8 (6.2)	36.4 (6.1)
Redundancy[a]	21.6 (17.7)	10.7 (11.0)	10.6 (10.6)
Refinement statistics			
Resolution range (Å)	19.85–1.65	19.98–1.90	19.67–1.80
No. of monomer/asymmetric unit	1	1	1
R_{fact}/R_{free} (%)[c,d]	15.1/17.3	15.9/18.8	16.0/19.0
RMSD bond length (Å)[e]	0.012	0.014	0.012
RMSD bond angles (°)[e]	1.279	1.295	1.199
No. of atoms	3749	3576	3697
Average *B*-factor (Å^2)	16.8	16.6	20.1

[a] The values in parentheses are for the highest resolution shell.
[b] $R_{merge} = \Sigma\Sigma|I - <I>|/\Sigma I$.
[c] $R_{fact} = \Sigma||F_o| - k|F_c||/\Sigma|F_o|$, where F_o and F_c are the observed and calculated structure factor amplitudes, respectively.
[d] R_{free} was calculated as the R_{fact} for 5% of the reflections that were not included in the refinement.
[e] RMSD, root mean square deviation.

WHAT-IF (46) and PROCHECK (47). X-ray diffraction data sets of the L78F and F288G mutants were collected using a beam line BL26B1 instrument equipped with an ADSC Quantum 210 CCD detector at SPring-8. The structures of L78F and F288G were solved using a molecular replacement method using MOLREP (48), followed by refinement using COOT and REMAC5. The final refinement statistics are summarized in Table 1.

Structural Analysis of $P450_{SP\alpha}$ and $P450_{BS\beta}$—Electrostatic potentials were calculated using GRASP2 (49). Probe-occupied voids were calculated using VOIDOO (50), and a probe of 1.1 Å and a grid mesh of 0.3 Å were used unless otherwise specified. The accessible channels were calculated using CAVER (51). All of the protein figures were depicted using PyMOL (52).

Hydroxylation of Myristic Acid—The standard reaction mixture contained 0.1 M potassium phosphate (pH 7.0), 0–120 μM myristic acid (C_{14}) (0–60 μM for F288G and A172F/F288G), 50 nM $P450_{SP\alpha}$ or $P450_{BS\beta}$, and 200 μM H_2O_2 in a total volume of 1 ml. The reaction mixture was incubated at 37 °C for 1 min, and then the reaction was quenched by adding 500 μl of dichloromethane followed by vigorous mixing. After the addition of 12-hydroxydodecanoic acid as an internal standard, the products were extracted with dichloromethane. For derivatization of the extract, 50 μl of *N*,*O*-bis(trimethylsilyl)trifluoroacetamide (BSTFA) containing 1% (v/v) trimethylchlorosilane (TMCS) was added, and the mixture was incubated in the dark at room temperature for 2 h. The derivatized products were analyzed using a Shimadzu GC-17A (Shimadzu Corp., Kyoto, Japan) equipped with a Shimadzu GC/MS-QP5000 and Rxi™-5ms capillary column (30 m × 0.25 mm; Restek Corp., Bellefonte, PA) to identify the products. The GC/MS analytical conditions were as follows: column temperature, 50 °C (1 min) to 40 °C/min (5 min) to 250 °C (8 min); injection temperature, 250 °C; interface temperature, 280 °C; carrier gas, helium; flow rate, 0.9 ml/min, mode, split mode; and split ratio, 1/50. To quantify the products, derivatization of the extract was performed by adding 9-anthryldiazomethane and incubating the solution in the dark at room temperature for 1 h. For quantification of the products, reverse phase HPLC analysis was performed using an Inertsil® ODS-3 column (4.6 mm × 250 mm; GL Sciences, Inc., Tokyo, Japan) installed on a Shimadzu SCL-$10A_{VP}$ system controller equipped with Shimadzu LC-$10AD_{VP}$ pump systems, a Shimadzu RF-$10A_{XL}$ fluorescence spectrometer, a Shimadzu CTO-$10A_{VP}$ column oven, and a Shimadzu DGU-12A degasser. The HPLC analytical conditions were as follows: flow rate, 1.0 ml/min; acetonitrile/water = 99/1; column temperature, 30 °C; excitation wavelength, 365 nm, emission wavelength, 412 nm; and retention times, 12-hydroxydodecanoic acid (6.41 min), β-OH C_{14} (10.7 min), α-OH C_{14} (11.9 min), and C_{14} (21.5 min). Chiral separation of the products was performed on a CHIRALPAK AD-RH column (Daicel Chemical Industries, Ltd., Osaka, Japan) installed on the same reverse phase HPLC system as in the case of the quantification. The absolute configuration was assigned by comparison of the product ratios in the hydroxylation of C_{14} by $P450_{SP\alpha}$ WT (53) and $P450_{BS\beta}$ WT (54). The HPLC conditions for the chiral separation were as follows: flow rate, 0.9 ml/min; linear gradient, MeOH/water = 85/15 (0–10 min) to 100/0 (100–120 min); column temperature, 40 °C; excitation, 365 nm; emission, 412 nm; retention times, (*R*)-α-OH C_{14} (34.2 min), (*S*)-α-OH C_{14} (37.6 min), (*S*)-β-OH C_{14} (49.8 min), and (*R*)-β-OH C_1 (53.2 min).

UV-visible and EPR Measurements—UV-visible spectra were recorded using a Shimadzu UV-2400 PC spectrophotometer at room temperature. X-band EPR spectra were recorded using an E500 X-band CW-EPR instrument (Bruker, Ettlingen, Germany) at 10 K. A cryostat (ITC503; Oxford Instruments Co., Abingdon, UK) was used for measurements at low temperatures.

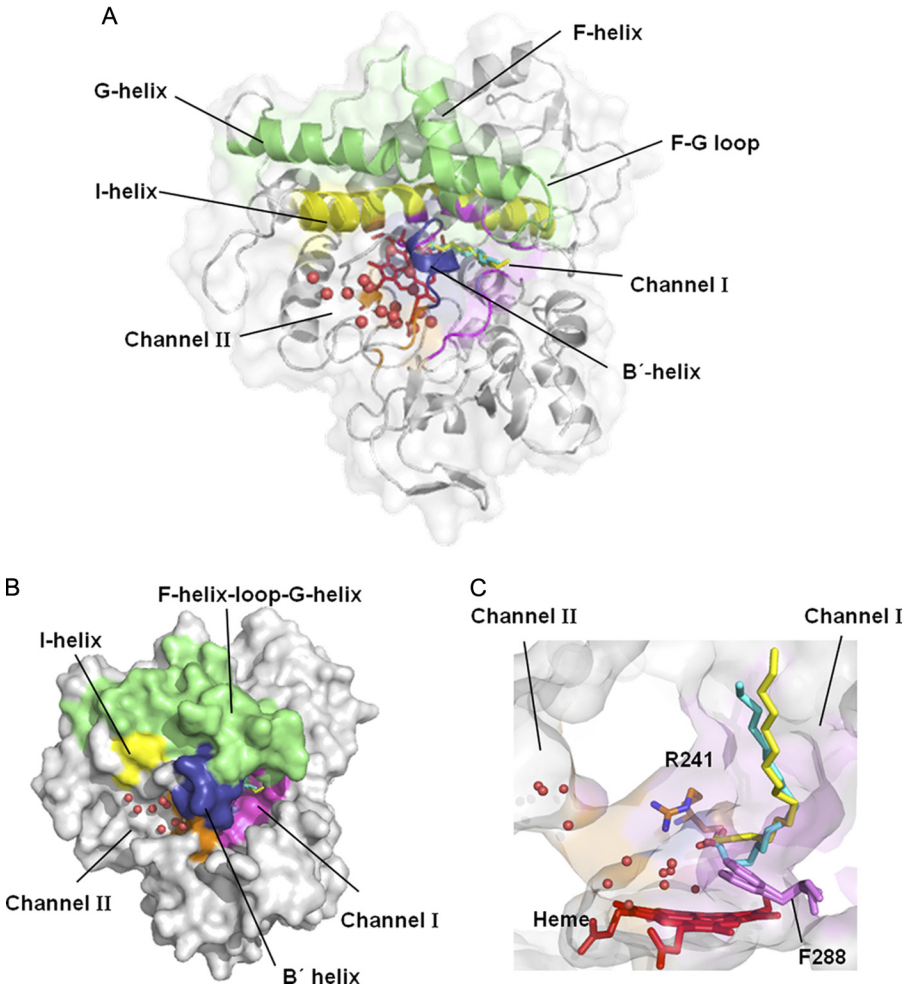

FIGURE 1. **Overall structure of $P450_{SP\alpha}$ with palmitic acid.** The B′ helix and F helix-loop-G helix are colored in *blue* and *green*, respectively. Heme (*red*) and palmitic acid (*yellow* and *cyan*) are represented as *stick models*. The Channel I (*magenta*) and Channel II (*orange*) locations were calculated using CAVER (51). Water molecules in Channel II are represented as *red spheres*. *A*, the distal face of $P450_{SP\alpha}$. *B*, surface model of $P450_{SP\alpha}$. *C*, two channels of $P450_{SP\alpha}$. Arg^{241} (*orange*) and Phe^{288} (*purple*) are labeled.

RESULTS AND DISCUSSION

Overall Structure and Substrate Binding—The structure of $P450_{SP\alpha}$ was resolved at a resolution of 1.65 Å (Fig. 1). One molecule was observed in the asymmetric unit. The overall structure exhibited typical P450 folding with 17 α helices and three β sheets. It has a trigonal prism-shaped structure with the heme buried deep inside the protein. The I helix lays across the interior of the P450 molecule on the distal side of the heme group. Two channels connecting the active site cavity with the protein surface were identified (Fig. 1). Channel I is composed of hydrophobic residues (Ile^{73}, Leu^{77}, Leu^{78}, Phe^{169}, Ala^{172}, Ala^{245}, Phe^{287}, Phe^{288}, Pro^{289}, Leu^{398}, and Pro^{399}) (Fig. 2*A*). Channel II includes hydrophilic residues (Gln^{84} and Asn^{238}) as its constituent residues. A cluster of water molecules with a hydrogen-bonding network was observed in Channel II (Fig. 2*D*). We expect that Channel II would be used for the ingress of H_2O_2 and the egress of water during the reaction. Phe^{288} is located at the border of the two channels, but the two channels are not clearly separated because the entrances of the channels are wide (Figs. 1, *B* and *C*, and 3*A*).

Although no substrates were added to the purified $P450_{SP\alpha}$, the initial $2F_o - F_c$ electron density map showed a long continuous electron density in Channel I (Fig. 2*A*). One of the ends of this electron density, located near Arg^{241} in the active site, has a Y-shape. Because the shape of this electron density is very similar to that of a long alkyl chain fatty acid observed in P450BM3 (21) and $P450_{BS\beta}$ (30), we assumed that this electron density corresponds to a long alkyl chain fatty acid originating from *Escherichia coli* cells (55). Indeed, GC/MS analysis of the extract of the purified $P450_{SP\alpha}$ with dichloromethane showed that palmitic acid and stearic acid were coexistent, even after purification (supplemental Fig. S1). It was difficult to deduce the length of the alkyl chain of the fatty acid based on the electron density of the substrate(s) because the electron density of the substrate was shorter than the alkyl chain of palmitic acid, possibly because of disordering. Therefore, we tentatively assigned this electron density to palmitic acid. In addition, because the Y-shaped electron density adjacent to the Arg^{241} was accompanied by an additional electron density, two alternative conformations with occupancies of 0.7 (Conformation A) and 0.3 (Conformation B) were placed and refined (Fig. 2, *B* and *C*). The terminal alkyl chain of palmitic acid in the final structure is highly disordered, indicating that the terminal alkyl chain is loosely fixed. It is noteworthy that the A′-helix, B′-he-

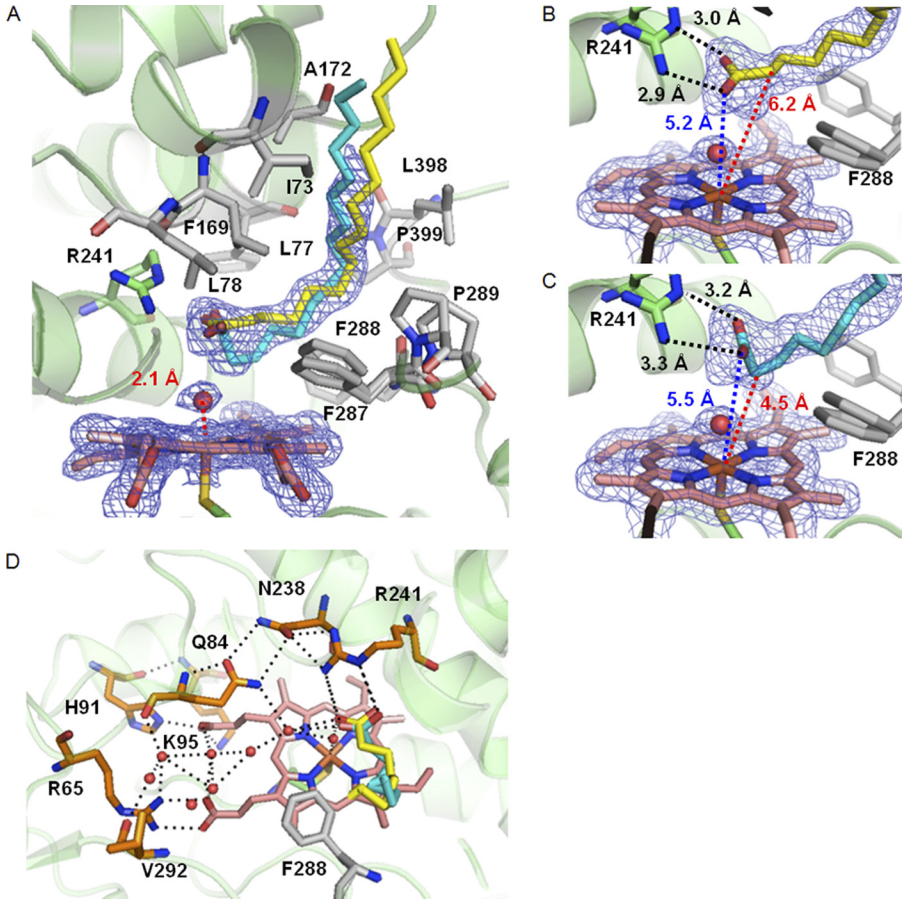

FIGURE 2. **The heme cavity of P450$_{SP\alpha}$.** The $2F_o - F_c$ electron density maps of heme, palmitic acid, and a water molecule coordinated to the iron are contoured at the 1 σ level (*blue mesh*). The hydrophobic amino acid residues, heme, and Cys[361] are represented as *stick models*. A water molecule coordinated to the iron is represented by a *red sphere*. The distance between the iron and water is shown in *red*. *A*, two alternative conformations of palmitic acid shown as *yellow* and *cyan stick models*. *B*, palmitic acid with 0.7 occupancy (Conformation A). *C*, palmitic acid with 0.3 occupancy (Conformation B). The interaction of Arg[241] with the oxygen atoms of the carboxylate group of palmitic acid are shown as *black dashed lines*. The distance of the C_α carbon and the oxygen atoms of palmitic acid from the iron and are shown as *red dashed lines* and *blue dashed lines*, respectively. *D*, hydrogen bond network in Channel II of P450$_{SP\alpha}$. Heme (*pink*), palmitic acid (*yellow and cyan*), and hydrophilic residues and Val[292] (*orange*) are represented as *stick models*. Water molecules are represented as *red spheres*. Hydrogen bonds are shown as *dashed lines*.

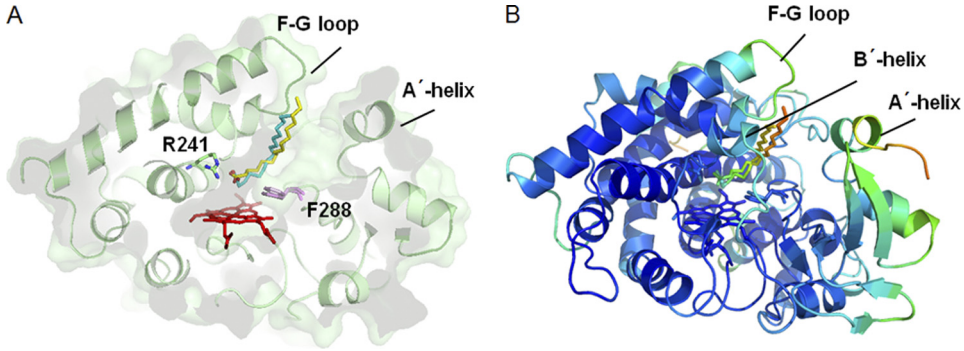

FIGURE 3. **The substrate access channel of P450$_{SP\alpha}$.** *A*, the substrate access channel (Channel I) of P450$_{SP\alpha}$. Heme, palmitic acid, Arg[241], and Phe[288] are represented as *stick models*. *B*, *B*-factor of P450$_{SP\alpha}$.

lix, and F–G loop have relatively high *B*-factors (Fig. 3*B*) and that the entrance of Channel I is open wide (Fig. 3*A*), suggesting that this region is flexible even though the substrate was accommodated. The substrate access channel and *B*-factor of P450$_{BS\beta}$ are shown in supplemental Fig. S2 for comparison.

The charge distribution on the surfaces of the proximal and distal sides of P450$_{SP\alpha}$ is shown in Fig. 4. In contrast to the charge distribution typical of P450s such as P450BM3 (56, 57), negative surface charges were observed on the proximal side of P450$_{SP\alpha}$. A positive surface potential on the proximal side of regular P450 is important for the recognition of reductases in the electron transfer step of oxygen activation in the P450 catalytic cycle (58). The negative surface potential on the proximal side of P450$_{SP\alpha}$ may preclude binding of a reductase. This unique charge potential distribution of P450$_{SP\alpha}$ is an indication that P450$_{SP\alpha}$ does not need binding of a reductase and prefers

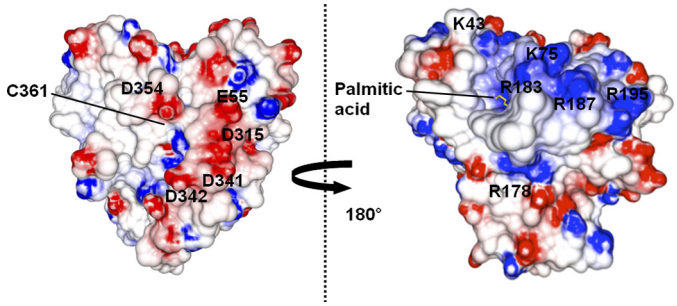

FIGURE 4. **Electrostatic potential surface of $P450_{SP\alpha}$.** Electrostatic surfaces of $P450_{SP\alpha}$ were calculated using GRASP2 (49). The negatively charged surface is represented in *red*, and the positively charged surface is represented in *blue*. Palmitic acid is shown as a *yellow stick model*.

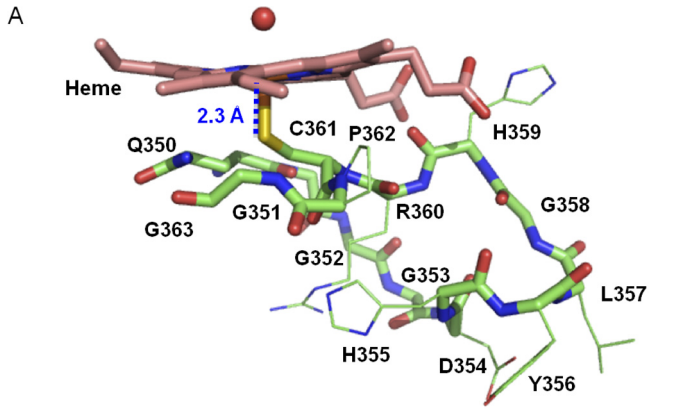

B

CYP152B1 ($P450_{SP\alpha}$)	Q G G G **D** H Y L - - - - - G H R **C** P G
CYP152A1 ($P450_{BS\beta}$)	Q G G G **H** A E K - - - - - G H R **C** P G
CYP74A (AOS)	W S N **G** P E T E T P T V G N K Q **C** A G
CYP101A1 (P450cam)	F G H **G** - - - - - - - - - S H L **C** L G
CYP102A1 (P450BM3)	F G N **G** - - - - - - - - - Q R A **C** L G

FIGURE 5. **The proximal side of the heme of $P450_{SP\alpha}$.** *A*, the main chain composed of the loop at the proximal side of the heme is represented as a *green stick model*. Heme is shown as a *pink stick model*. The water molecule on the heme is represented as a *red sphere*. The distances between the heme iron and nitrogen atoms of the main chain from the sulfur atom of Cys^{361} are shown in *blue*. *B*, comparison of the amino acid sequence of $P450_{SP\alpha}$ with other P450s. Conserved amino acid residues are depicted in *bold type*.

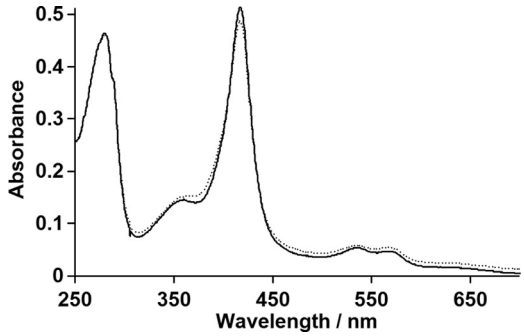

FIGURE 6. **UV-visible absorption spectra of $P450_{SP\alpha}$.** The spectra of $P450_{SP\alpha}$ in 0.1 M potassium phosphate buffer (pH 7.0) containing 0.3 M KCl and 20% (v/v) glycerol in the absence (*solid line*) and presence of 120 μM of myristic acid (*dotted line*). The concentration of $P450_{SP\alpha}$ was 3.1 μM.

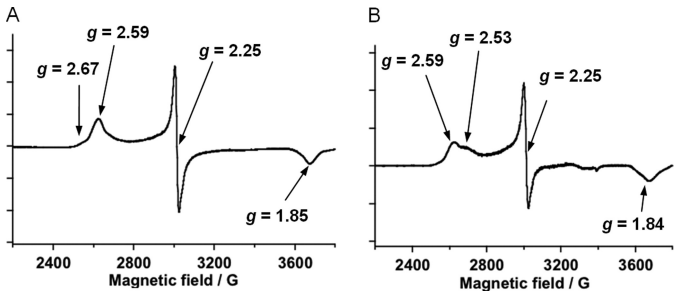

FIGURE 7. **EPR spectra of $P450_{SP\alpha}$ recorded at 10 K.** The spectra of $P450_{SP\alpha}$ in the absence (*A*) and presence of 120 μM of myristic acid (*B*) are shown. The concentrations of $P450_{SP\alpha}$ were 44 and 24 μM for the substrate-free form and for the myristic acid-bound form, respectively.

the H_2O_2 shunt pathway. $P450_{BS\beta}$ also has no positively charged region on the surface of the proximal side. In addition, a long loop structure was observed on the proximal side (^{349}QGGGDHYLGHRC^{361}) (Fig. 5), whereas P450s that require electron transfer from reductases have short loop structures. $P450_{cam}$, for example, has a short loop structure, ^{350}FGHGSHLC^{357}. $P450_{BS\beta}$ (^{352}QGGGHAEKGHRC^{363}) (30) and allene oxide synthase (^{455}WSNGPETETPTVGNKQC^{472}) (59) also have long loop structures at the proximal side of the heme, implying that the long loop structure is a common feature among P450s that do not require electron transfer systems for the activation of molecular oxygen.

Active Site Structure—At the active site, Arg^{241} is located above the heme, and its guanidinium group interacts with the carboxylate group of palmitic acid (Fig. 2*A*); the distances between two oxygen atoms of the carboxylate group and the guanidinium group of Arg^{241} ($N_{\eta 2}$ and N_{ϵ}) are 2.9 and 3.0 Å in Conformation A (Fig. 2*B*) and 3.3 and 3.2 Å in Conformation B (Fig. 2*C*), respectively. In contrast to other heme enzymes that utilize H_2O_2, $P450_{SP\alpha}$ lacks general acid-base residues around the distal side of the heme. As an alternative, the terminal carboxylate group of palmitic acid is located above the heme. The distance between the oxygen atoms close to the heme iron is 5.2 Å for Conformation A and 5.5 Å for Conformation B, indicating that the location of the oxygen atom is similar to that of the glutamic acid moiety of CPO (34, 35) and that of the terminal carboxylate group of palmitic acid observed in $P450_{BS\beta}$. These observations indicate that participation of the terminal carboxylate group of the fatty acid in the generation of active species using H_2O_2 (Scheme 1) is common among H_2O_2-dependent P450s. The distal side of the heme is hydrophilic because of Gln^{84}, Asp^{238}, Arg^{241}, and the carboxylate group of palmitic acid (Fig. 2*D*). The polar environment is expected to facilitate the heterolytic cleavage of the O–O bond of H_2O_2 to generate compound I, as is proposed for heme peroxidases such as cytochrome *c* peroxidase (31, 32), HRP (33), CPO (34, 35), and myoglobin mutants (60, 61). A water molecule is located 2.1 Å away from the heme iron and could function as a sixth ligand on the heme even though the palmitic acid occupies the distal side of the heme cavity (Fig. 2*A*). The UV-visible spectra of $P450_{SP\alpha}$ in the absence and presence of 120 μM of myristic acid showed a Soret absorption peak at 417 nm, which is consistent with a typical six-coordinate low-spin ferric heme (Fig. 6). The EPR spectrum of the substrate-free form of $P450_{SP\alpha}$ showed a ferric low spin state having *g* value 2.59 (g_z), 2.25 (g_y), and 1.85 (g_x) (Fig. 7), suggesting that the electronic environment of the heme iron of $P450_{SP\alpha}$ resembles that of CPO (2.61 (g_z), 2.26 (g_y), 1.83

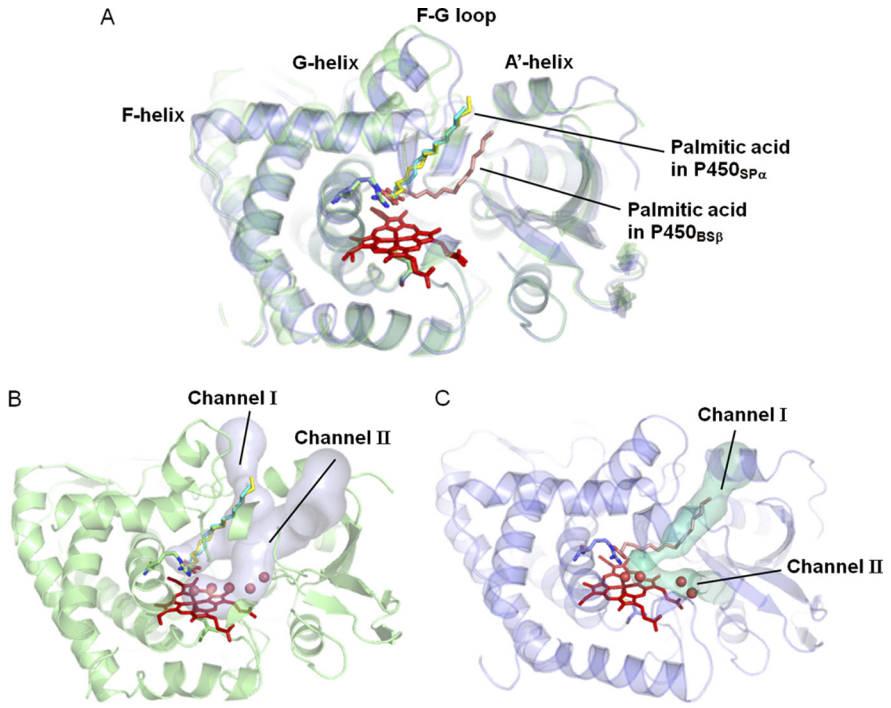

FIGURE 8. **Overall structure of $P450_{SP\alpha}$ superposed on that of $P450_{BS\beta}$.** *A*, the superposition of the structures. The structures of $P450_{SP\alpha}$ and $P450_{BS\beta}$ are represented in *green* and *blue*, respectively. Heme is depicted as a *red stick model*. Palmitic acids in $P450_{SP\alpha}$ and $P450_{BS\beta}$ are represented as a *yellow* and *cyan stick models* and a *pink stick* model, respectively. *B* and *C*, substrate access channel location of $P450_{SP\alpha}$ (*B*) and $P450_{BS\beta}$ (*C*) calculated using CAVER (51) are shown as a *light blue* surface for $P450_{SP\alpha}$ and a *cyan* surface for $P450_{BS\beta}$.

(g_x), pH 5.2) (62) rather than those of bacterial P450s such as $P450_{cam}$ (2.45 (g_z), 2.26 (g_y), 1.91 (g_x)) (63) and P450BM3 (2.42 (g_z), 2.26 (g_y), 1.92 (g_x)) (64). The EPR spectral change of $P450_{SP\alpha}$ upon addition of myristic acid (120 μM) was very small, indicating that the low spin state is essentially retained irrespective of substrate binding. Minor signals at $g = 2.67$ in the substrate free-form and at $g = 2.53$ in the myristic acid-bound form might reflect P420 species of $P450_{SP\alpha}$ (supplemental Fig. S5), whereas signals are different from that of P420 species of $P450_{cam}$ (2.46 (g_z)) (64).

Regioselectivity for Hydroxylation of Fatty Acid—$P450_{SP\alpha}$ exclusively catalyzes the hydroxylation of fatty acid at the C_α position and produces the corresponding α-hydroxy fatty acid, whereas $P450_{BS\beta}$ produces α and β hydroxy products in the ratio of 43:57. In the crystal structure of $P450_{SP\alpha}$, the distances of the C_α carbon and the C_β carbon in Conformation B from the heme iron are 4.5 and 5.5 Å, respectively. Because the C_α carbon in Conformation B is clearly close to the iron atom, and the distance of 4.5 Å agrees well with the distance between the C5 position of *d*-camphor and the heme iron in $P450_{cam}$ (65), Conformation B is expected to produce the α-hydroxy fatty acid selectively. Because the C_α and C_β carbons in Conformation A are both far away from the heme iron in respect of the hydroxylation reaction, we assume that Conformation A is a nonproductive conformation. In the crystal structure of $P450_{BS\beta}$, the C_α and C_β carbons of palmitic acid are located at distances of 5.0 and 6.2 Å from the heme iron, respectively. The substrate observed in $P450_{BS\beta}$ needs to be closer to the heme iron to be hydroxylated, as was observed for P450BM3 (66). The C_α and C_β carbons of the possible productive conformation of palmitic acid in $P450_{BS\beta}$ may be equally close to the heme iron.

Structural Comparison of $P450_{SP\alpha}$ with $P450_{BS\beta}$—To gain further insight into H_2O_2-dependent P450s, the structure of $P450_{SP\alpha}$ was compared with that of $P450_{BS\beta}$. The structure of $P450_{SP\alpha}$ is superimposed on that of $P450_{BS\beta}$ in Fig. 8. Except for the B′ helix and the F–G loop, the overall structures are well superposed with a root mean square deviation value of 1.4 Å. The locations of Channel I are notably different, resulting in different locations for the bound palmitic acid. The palmitic acid is more perpendicular to the heme plane in $P450_{SP\alpha}$ than in $P450_{BS\beta}$. The active site cavity of $P450_{SP\alpha}$ is smaller than that of $P450_{BS\beta}$ (supplemental Fig. S3). The smaller active site cavity is mainly due to the presence of Phe^{288} in the heme cavity of $P450_{SP\alpha}$. The corresponding amino acid residue in $P450_{BS\beta}$ is Gly^{290}. The effect of Phe^{288} and the location of Channel I are discussed in the next section.

Hydroxylation of Myristic Acid by Mutants—We carried out mutagenesis study to elucidate the structural requirement for the α-selective reaction of $P450_{SP\alpha}$. Based on the comparison between amino acid residues in the active sites of $P450_{SP\alpha}$ and $P450_{BS\beta}$, two amino acid residues in the active site of $P450_{SP\alpha}$, Phe^{288} and Leu^{78}, were mutated to the corresponding $P450_{BS\beta}$ residues and vice versa. The active site cavity of $P450_{SP\alpha}$ is smaller than that of $P450_{BS\beta}$, mainly because of the side chain of Phe^{288} (supplemental Fig. S3), which interacts directly with the fatty acid. Although Leu^{78} does not interact with the fatty acid, it is located at the border of the channels and may affect the catalytic reaction. Three mutants of $P450_{SP\alpha}$, L78F, F288G, and L78F/F288G, and three $P450_{BS\beta}$ mutants, F79L, G290F, and F79L/G290F, were prepared and their catalytic activities, regioselectivities, and stereoselectivities were examined (Table 2). $P450_{BS\beta}$ mutants F79L and G290F had 75 and 95% α selectivity,

TABLE 2
Hydroxylation of myristic acid by $P450_{SP\alpha}$ and $P450_{BS\beta}$

Enzyme	k_{cat}	K_m	Regioselectivity	Stereoselectivity	
				At α-position (R):(S)	At β-position (R):(S)
	nmol/min/nmol P450	*μM*	*α-OH %*		
$P450_{SP\alpha}$WT	1300 ± 20	43 ± 2	>99	3:97	
$P450_{SP\alpha}$L78F	5500 ± 930	300 ± 70	>99	4:96	
$P450_{SP\alpha}$F288G	770 ± 70	100 ± 20	>99	19:81	
$P450_{SP\alpha}$L78F/F288G	1300 ± 40	85 ± 16	>99	21:79	
$P450_{SP\alpha}$A172F	1200 ± 20	68 ± 3	>99	3:97	
$P450_{SP\alpha}$A172F/F288G	100 ± 2	23 ± 2	>99	17:83	
$P450_{BS\beta}$WT	1400 ± 180	66 ± 20	43	76:24	98:2
$P450_{BS\beta}$F79L	1400 ± 30	54 ± 3	75	62:38	99:1
$P450_{BS\beta}$G290F	1900 ± 210	190 ± 30	95	29:71	85:15
$P450_{BS\beta}$F79L/G290F	890 ± 20	95 ± 3	77	28:72	86:14

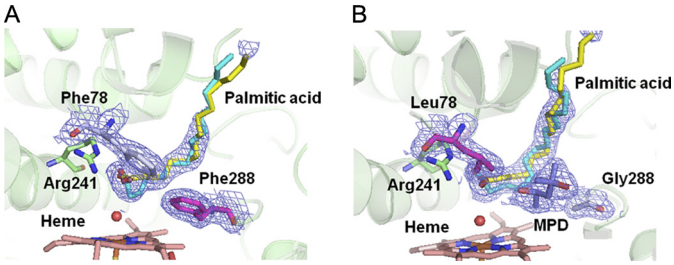

FIGURE 9. **The active site structures of $P450_{SP\alpha}$ L78F (*A*) and F288G (*B*).** Palmitic acid, heme, Arg^{241}, Phe^{78} or Leu^{78}, Phe^{288} or Gly^{288}, and MPD are represented as stick models. A water molecule coordinated to the iron is represented as a *sphere*. The $2F_o - F_c$ electron density maps of palmitic acid, Phe^{78} or Leu^{78}, Phe^{288} or Gly^{288}, and MPD are contoured at the 1 σ level (*blue mesh*). The position of Phe^{288} in the WT is occupied by MPD in F288G. In both structures, palmitic acid with 0.7 occupancy and 0.3 occupancy are colored *yellow and cyan*, respectively.

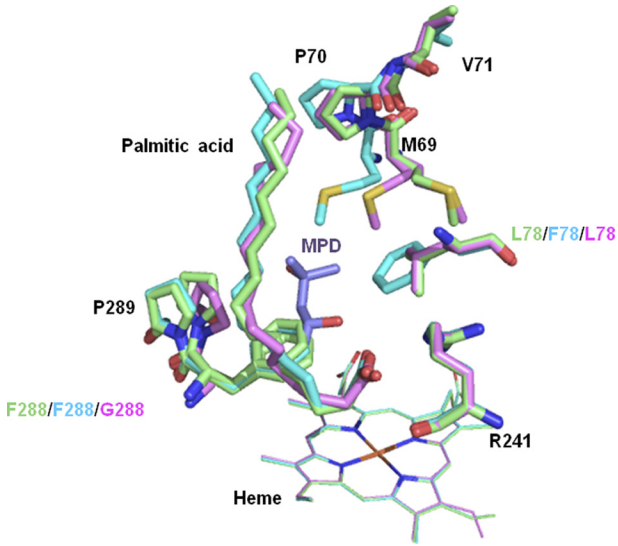

FIGURE 10. **Comparison of WT (*green*), L78F (*cyan*), and F288G (*purple*).** Superimposition of two mutants and WT $P450_{SP\alpha}$. Side view from the opposite side of the propionate of the heme. Heme is represented as a line. MPD in F288G is represented as a blue stick model. Root mean square deviation values over 9–415 amino acid residues of C_α atoms are 0.225 for L78F and 0.197 for F288G, respectively.

respectively, indicating that the regioselectivity of $P450_{BS\beta}$ was greatly altered. The substitution of Gly^{290} with Phe must induce a conformational change in myristic acid, and the C_α carbon is expected to move closer than the C_β carbon to the heme iron. In sharp contrast with the $P450_{BS\beta}$ mutants, no clear differences in regioselectivity were observed for $P450_{SP\alpha}$ mutants, whereas the amino acids at the active site were replaced with the corresponding amino acids of $P450_{BS\beta}$, which has β-regioselectivity. Three mutants of $P450_{SP\alpha}$ showed >99% α selectivity. To further investigate the regioselectivity of $P450_{SP\alpha}$, two mutants of $P450_{SP\alpha}$, A172F and A172F/F288G, were prepared. Ala^{172} located in the F–G loop seems to be important for controlling fatty acid conformation. However, the regioselectivity was not affected by these mutagenesis experiments, indicating that the mutagenesis at the active site and at the F–G loop does not alter the position of bound palmitic acid. The x-ray crystal structures of the L78F and F288G mutants revealed that there is little difference in the location of the bound palmitic acid in Conformation B (the productive conformation) and the location of the hydrophilic channel (Fig. 9), whereas the position of the amino acids located near the active site, Met^{69}, Pro^{70}, and Pro^{289}, are shifted (Fig. 10 and supplemental Fig. S4). The C_α positions of palmitic acid in both mutants are essentially the same as in the WT. Whereas the stereoselectivity of α hydroxylation of myristic acid was slightly reduced by mutagenesis (Table 2), the regioselectivity of $P450_{SP\alpha}$ was not affected, suggesting that the small perturbation induced by the mutagenesis is insufficient to alter the high regioselectivity of $P450_{SP\alpha}$. We presume that the regioselectivity of $P450_{SP\alpha}$ is highly controlled by its hydrophobic channel. The orientation of the channel (almost perpendicular to the heme plane) and the wide open entrance appear to be crucial for the high α-selectivity of hydroxylation. The hydrophobic channel may control the direction of the fatty acid access. Further mutagenesis studies, especially at the F and G helices and at the F–G loop region, are necessary for elucidating the mechanistic details of the highly selective α-hydroxylation of fatty acid catalyzed by $P450_{SP\alpha}$.

Conclusion—We have determined the x-ray crystal structure of H_2O_2-dependent $P450_{SP\alpha}$ as a palmitic acid-bound form at a resolution of 1.65 Å. The crystal structure revealed that the carboxylate group of the fatty acid interacts with Arg^{241}, which is located above the heme. Previous studies on the reaction mechanism of $P450_{BS\beta}$ suggested that the carboxylate group of the fatty acid serves as a general acid-base catalyst for the generation of compound I using H_2O_2. Our crystal structure study confirms that this substrate-assisted activation mechanism is also conserved in $P450_{SP\alpha}$, indicating that the substrate-assisted activation mechanism is common in the H_2O_2-dependent P450-catalyzed hydroxylation reaction with fatty acids. Notably, a water molecule was observed as the sixth ligand of the heme iron, even in the presence of palmitic acid. Consistent

with the crystal structure, the ferric low spin state of $P450_{SP\alpha}$ was retained irrespective of the substrate binding. These results also indicate that the shift in redox potential of the heme that is induced by substrate binding, which is generally indispensable for the reductive activation of molecular oxygen, is not essential for the H_2O_2-dependent P450s. Crystallographic studies on substrate binding revealed that the C_α carbon of the bound palmitic acid in Conformation B is situated close to the heme iron (4.5 Å). This conformation explains the highly selective α-hydroxylation of fatty acid. Surprisingly, mutations at the active site and at the F–G loop of $P450_{SP\alpha}$ did not impair the high regioselectivity. The crystal structures of the L78F and F288G mutants revealed that the location of the bound palmitic acid was not affected by these mutations. These results imply that the orientation of the hydrophobic channel of $P450_{SP\alpha}$, which is more perpendicular to the heme plane than that of $P450_{BS\beta}$, is crucial for the highly selective α-hydroxylation. Although further mutagenesis studies are required to fully understand the high regioselectivity of $P450_{SP\alpha}$, the structural studies reported here contribute to a better understanding of the relationship between the structure and function of H_2O_2-dependent P450s at the atomic level.

Acknowledgments—We thank Dr. Go Ueno, Dr. Hironori Murakami, Dr. Masatomo Makino, and Dr. Nobuyuki Shimizu for assistance with the data collection at SPring-8. We thank Dr. Isamu Matsunaga for the kind gift of the expression system of $P450_{SP\alpha}$.

REFERENCES

1. Ortiz de Montellano, P. R. (2005) *Cytochrome P450: Structure, Mechanism, and Biochemistry*, 3rd, ed., Plenum, New York
2. Guengerich, F. P. (2008) *Chem. Res. Toxicol.* **21,** 70–83
3. Denisov, I. G., Makris, T. M., Sligar, S. G., and Schlichting, I. (2005) *Chem. Rev.* **105,** 2253–2277
4. Sono, M., Roach, M. P., Coulter, E. D., and Dawson, J. H. (1996) *Chem. Rev.* **96,** 2841–2888
5. Poulos, T. L., Finzel, B. C., Gunsalus, I. C., Wagner, G. C., and Kraut, J. (1985) *J. Biol. Chem.* **260,** 16122–16130
6. Williams, P. A., Cosme, J., Sridhar, V., Johnson, E. F., and McRee, D. E. (2000) *Mol. Cell* **5,** 121–131
7. Williams, P. A., Cosme, J., Ward, A., Angove, H. C., Matak Vinković, D., and Jhoti, H. (2003) *Nature* **424,** 464–468
8. Williams, P. A., Cosme, J., Vinkovic, D. M., Ward, A., Angove, H. C., Day, P. J., Vonrhein, C., Tickle, I. J., and Jhoti, H. (2004) *Science* **305,** 683–686
9. Wester, M. R., Yano, J. K., Schoch, G. A., Yang, C., Griffin, K. J., Stout, C. D., and Johnson, E. F. (2004) *J. Biol. Chem.* **279,** 35630–35637
10. Yano, J. K., Hsu, M. H., Griffin, K. J., Stout, C. D., and Johnson, E. F. (2005) *Nat. Struct. Mol. Biol.* **12,** 822–823
11. Mast, N., White, M. A., Bjorkhem, I., Johnson, E. F., Stout, C. D., and Pikuleva, I. A. (2008) *Proc. Natl. Acad. Sci. U.S.A.* **105,** 9546–9551
12. Scott, E. E., He, Y. A., Wester, M. R., White, M. A., Chin, C. C., Halpert, J. R., Johnson, E. F., and Stout, C. D. (2003) *Proc. Natl. Acad. Sci. U.S.A.* **100,** 13196–13201
13. Scott, E. E., White, M. A., He, Y. A., Johnson, E. F., Stout, C. D., and Halpert, J. R. (2004) *J. Biol. Chem.* **279,** 27294–27301
14. Porubsky, P. R., Meneely, K. M., and Scott, E. E. (2008) *J. Biol. Chem.* **283,** 33698–33707
15. Yano, J. K., Koo, L. S., Schuller, D. J., Li, H., Ortiz de Montellano, P. R., and Poulos, T. L. (2000) *J. Biol. Chem.* **275,** 31086–31092
16. Park, S. Y., Yamane, K., Adachi, S., Shiro, Y., Weiss, K. E., Maves, S. A., and Sligar, S. G. (2002) *J. Inorg. Biochem.* **91,** 491–501
17. Oku, Y., Ohtaki, A., Kamitori, S.,Nakamura, N., Yohda, M., Ohno, H., and Kawarabayasi, Y. (2004) *J. Inorg. Biochem.* **98,** 1194–1199
18. Poulos, T. L., Finzel, B. C., and Howard, A. J. (1987) *J. Mol. Biol.* **195,** 687–700
19. Lee, Y. T., Wilson, R. F., Rupniewski, I., and Goodin, D. B. (2010) *Biochemistry* **49,** 3412–3419
20. Ravichandran, K. G., Boddupalli, S. S., Hasermann, C. A., Peterson, J. A., and Deisenhofer, J. (1993) *Science* **261,** 731–736
21. Li, H., and Poulos, T. L. (1997) *Nat. Struct. Biol.* **4,** 140–146
22. Hasemann, C. A., Ravichandran, K. G., Peterson, J. A., and Deisenhofer, J. (1994) *J. Mol. Biol.* **236,** 1169–1185
23. Cupp-Vickery, J. R., and Poulos, T. L. (1995) *Nat. Struct. Biol.* **2,** 144–153
24. Leys, D., Mowat, C. G., McLean, K. J., Richmond, A., Chapman, S. K., Walkinshaw, M. D., and Munro, A. W. (2003) *J. Biol. Chem.* **278,** 5141–5147
25. McLean, K. J., Lafite, P., Levy, C., Cheesman, M. R., Mast, N., Pikuleva, I. A., Leys, D., and Munro, A. W. (2009) *J. Biol. Chem.* **284,** 35524–35533
26. Podust, L. M., Poulos, T. L., and Waterman, M. R. (2001) *Proc. Natl. Acad. Sci. U.S.A.* **98,** 3068–3073
27. Makino, M., Sugimoto, H., Shiro, Y., Asamizu, S., Onaka, H., and Nagano, S. (2007) *Proc. Natl. Acad. Sci. U.S.A.* **104,** 11591–11596
28. Matsunaga, I., Kusunose, E., Yano, I., and Ichihara, K. (1994) *Biochem. Biophys. Res. Commun.* **201,** 1554–1560
29. Matsunaga, I., Yamada, M., Kusunose, E., Nishiuchi, Y., Yano, I., and Ichihara, K. (1996) *FEBS Lett.* **386,** 252–254
30. Lee, D. S., Yamada, A., Sugimoto, H., Matsunaga, I., Ogura, H., Ichihara, K., Adachi, S., Park, S. Y., and Shiro, Y. (2003) *J. Biol. Chem.* **278,** 9761–9767
31. Poulos, T. L., and Kraut, J. (1980) *J. Biol. Chem.* **255,** 8199–8205
32. Wang, J. M., Mauro, M., Edwards, S. L., Oatley, S. J., Fishel, L. A., Ashford, V. A., Xuong, N. H., and Kraut, J. (1990) *Biochemistry* **29,** 7160–7173
33. Gajhede, M., Schuller, D. J., Henriksen, A., Smith, A. T., and Poulos, T. L. (1997) *Nat. Struct. Biol.* **4,** 1032–1038
34. Sundaramoorthy, M., Terner, J., and Poulos, T. L. (1995) *Structure* **3,** 1367–1377
35. Sundaramoorthy, M., Terner, J., and Poulos, T. L. (1998) *Chem. Biol.* **5,** 461–473
36. Shoji, O., Fujishiro, T., Nakajima, H., Kim, M., Nagano, S., Shiro, Y., and Watanabe, Y. (2007) *Angew. Chem. Int. Ed. Engl.* **46,** 3656–3659
37. Shoji, O., Fujishiro, T., Nagano, S., Tanaka, S., Hirose, T., Shiro, Y., and Watanabe, Y. (2010) *J. Biol. Inorg. Chem.* **15,** 1331–1339
38. Otwinowski, Z., Borek, D., Majewski, W., and Minor, W. (2003) *Acta Crystallogr. A* **59,** 228–234
39. Sheldrick, G. M. (2008) *Acta Crystallogr. A* **64,** 112–122
40. Pape, T., and Schneider, T. R. (2004) *J. Appl. Crystallogr.* **37,** 843–844
41. Morris, R. J., Zwart, P. H., Cohen, S., Fernandez, F. J., Kakaris, M., Kirillova, O., Vonrhein, C., Perrakis, A., and Lamzin, V. S. (2004) *J. Synchrotron Radiat.* **11,** 56–59
42. Emsley, P., and Cowtan, K. (2004) *Acta Crystallogr. D Biol. Crystallogr.* **60,** 2126–2132
43. Brünger, A. T., Adams, P. D., Clore, G. M., DeLano, W. L., Gros, P., Grosse-Kunstleve, R. W., Jiang, J. S., Kuszewski, J., Nilges, M., Pannu, N. S., Read, R. J., Rice, L. M., Simonson, T., and Warren, G. L. (1998) *Acta Crystallogr. D Biol. Crystallogr.* **54,** 905–921
44. Winn, M. D., Murshudov, G. N., and Papiz, M. Z. (2003) *Methods Enzymol.* **374,** 300–321
45. Winn, M. D., Isupov, M. N., and Murshudov, G. N. (2001) *Acta Crystallogr. D Biol. Crystallogr.* **57,** 122–133
46. Vriend, G. (1990) *J. Mol. Graph.* **8,** 52–56
47. Lakowski, R., A., MacArthur, M. W., Moss, D. S., and Thornton, J. M. (1993) *J. Appl. Crystallogr.* **26,** 283–291
48. Vagin, A., and Teplyakov, A. (1997) *J. Appl. Crystallogr.* **30,** 1022–1025
49. Petrey, D., and Honig, B. (2003) *Methods Enzymol.* **374,** 492–509
50. Kleywegt, G. J., and Jones, T. A. (1994) *Acta Crystallogr. Sect. D* **50,** 178–185
51. Petrek, M., Otyepka, M., Banás, P., Kosinová, P., Koca, J., and Damborský, J. (2006) *BMC Bioinformatics* **7,** 316–325

52. DeLano, W. L. (2002) *The PyMOL Moleular Graphics System on World Wide Web*, DeLano Scientific, San Carlos, CA
53. Matsunaga, I., Ueda, A., Sumimoto, T., Ichihara, K., Ayata, M., and Ogura, H. (2001) *Arch. Biochem. Biophys.* **394,** 45–53
54. Matsunaga, I., Sumimoto, T., Ueda, A., Kusunose, E., and Ichihara, K. (2000) *Lipids* **35,** 365–371
55. Allen, E. E., and Bartlett, D. H. (2000) *J. Bacteriol.* **182,** 1264–1271
56. Sevrioukova, I. F., Li, H., Zhang, H., Peterson, J. A., and Poulos, T. L. (1999) *Proc. Natl. Acad. Sci. U.S.A.* **96,** 1863–1868
57. Yano, J. K., Blasco, F., Li, H., Schmid, R. D., Henne, A., and Poulos, T. L. (2003) *J. Biol. Chem.* **278,** 608–616
58. Nagano, S., Tosha, T., Ishimori, K., Morishima, I., and Poulos, T. L. (2004) *J. Biol. Chem.* **279,** 42844–42849
59. Lee, D. S., Nioche, P., Hamberg, M., and Raman, C. S. (2008) *Nature* **455,** 363–368
60. Ozaki, S., Matsui, T., and Watanabe, Y. (1997) *J. Am. Chem. Soc.* **119,** 6666–6667
61. Matsui, T., Ozaki, S., and Watanabe, Y. (1999) *J. Am. Chem. Soc.* **121,** 9952–9957
62. Hollenberg, P. F., Hager, L. P., Blumberg, W. E., and Peisach, J. (1980) *J. Biol. Chem.* **255,** 4801–4807
63. Lipscomb, J. D. (1980) *Biochemistry* **19,** 3590–3599
64. Miles, J. S., Munro, A. W., Rospendowski, B. N., Smith, W. E., McKnight, J., and Thomson, A. J. (1992) *Biochem. J.* **288,** 503–509
65. Li, H. Y., Narasimhulu, S., Havran, L. M., Winkler, J. D., and Poulos, T. L. (1995) *J. Am. Chem. Soc.* **117,** 6297–6299
66. Modi, S., Sutcliffe, M. J., Primrose, W. U., Lian, L. Y., and Roberts, G. C. K. (1996) *Nat. Struct. Biol.* **3,** 414–417